RSC Publishing Faraday Discussions

Light Harvesting and Energy Transfer in a Porphyrin-based Metal Organic Framework

Journal:	*Faraday Discussions*
Manuscript ID	FD-ART-11-2018-000194.R1
Article Type:	Paper
Date Submitted by the Author:	17-Dec-2018
Complete List of Authors:	Shaikh, Shaunak; Virginia Tech, Chemistry Chakraborty, Arnab; Virginia Tech, Chemistry Alatis, Jamie; Virginia Tech, Chemistry Cai, Meng; Virginia Tech, Chemistry Danilov, Evgeny; North Carolina State University, Department of Chemistry Morris, Amanda; Virginia Tech, Chemistry

Faraday Discussions

ARTICLE

Light Harvesting and Energy Transfer in a Porphyrin-based Metal Organic Framework

Received 00th January 20xx,
Accepted 00th January 20xx

DOI: 10.1039/x0xx00000x

www.rsc.org/

Shaunak M. Shaikh[a], Arnab Chakraborty[a], James Alatis[a], Meng Cai[a], Evgeny Danilov[b], Amanda J. Morris[a]*

We present synthesis and photophysical characterization of a water stable PCN-223(freebase) metal organic framework (MOF) constructed from meso-tetrakis(4-carboxyphenyl)porphyrin (TCPP). Photophysical properties of the synthesized crystalline material were studied by using a wide range of steady-state and time-resolved spectroscopic techniques. Quenching experiments performed on TCPP and PCN-223 demonstrated that the extent and the rate of quenching in MOF is significantly higher than monomeric ligand. Based on these results, we propose that upon photo-excitation, the singlet excitation energy migrates across neutral TCPP linkers until it is quenched by a N-protonated TCPP linker. The N-protonated linkers act as trap states that deactivate the excited state to the ground state. Variable temperature measurements aided in understanding the mechanism of singlet-singlet energy transfer in PCN-223 MOF. The rate of energy transfer and the total exciton hopping distance in PCN-223 were calculated to quantify the energy transfer characteristics of PCN-223. Nanosecond transient absorption spectroscopy was used to study the triplet excited state photophysics in both free ligand and PCN-223 MOF. Furthermore, femtosecond transient absorption spectroscopy was employed to get a better understanding of the photophysical processes taking place in ligand and MOF on ultrafast timescales. Efficient energy transfer (Förster radius = 54.5 Å) accompanied with long distance exciton hopping (173 Å) was obtained for PCN-223 MOF.

Introduction

One of the most important components of artificial photosynthesis assemblies are the antennae, which collect solar energy and direct it towards the reaction centers. A multi-chromophoric array with energy cascade can direct sequential photoexcited energy flow and perform the function of light harvesting antenna assemblies.[1] Multiporphyrin arrays been studied extensively with the aim of constructing antenna assemblies that mimic natural photosynthetic systems in terms of the efficiency of excitation energy transfer (EET). Subtle changes in structural parameters, such as connectivity, distance, and orientation between porphyrin units in the array can have strong implications on the nature of interchromophoric interactions, and the rates and efficiencies of EET.[2] Highlighted by highly-ordered crystal structures and synthetic tunability via crystal engineering, metal organic frameworks (MOFs) allow for precise control of distances and angles between chromophores and their alignment by judicious choice of ligands and metal nodes.[3–6] Porphyrin based MOFs are therefore ideal candidates to study EET as a function of structural parameters. Such studies will aid in the design of porphyrin-based architectures that are conducive for energy transfer. Before examining the role of MOF structure in EET, it is necessary to first understand the mechanistic aspects of EET and the factors that determine the efficiency of EET in porphyrin-based MOFs. To address these issues, we probed the energy transfer characteristics of PCN-223(fb), a Zr-MOF based on meso-tetrakis(4-carboxyphenyl)porphyrin (TCPP).

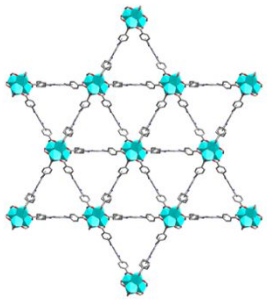

Figure 1. View of PCN-223(fb) along the c axis with uniform triangular 1D channels

Zr-TCPP MOFs have been studied extensively due to their exceptional chemical stability under harsh experimental conditions and their ability to exhibit a variety of functionalities like catalysis, light harvesting, gas-storage and sensing.[4,7–12] PCN-223, in particular, has a very unique structure (Fig. 1).[10] It consists of unprecedented D_{6h} symmetric $[Zr_6O_4(OH)_4]^{12+}$ nodes connected to 12 TCPP linkers, representing the first (4,12)-connected MOF with the "shp" topology. The closely-packed

[a] Department of chemistry, Virginia Tech, Blacksburg, Virginia, 24060, USA.
[b] Department of Chemistry, North Carolina State University, Raleigh, North Carolina, 27695-8204, USA.

† Electronic Supplementary Information (ESI) available: [Themogravimetric analysis, Nitrogen gas adsorption, spectral overlap calculation, steady state and nanosecond TA spectrum]. See DOI: 10.1039/x0xx00000x

structure of PCN-223 supports a high density of chromophores that can simultaneously absorb light and participate in the energy transfer process. The closest distance between two porphyrin struts is 10.71 Å (see supporting information, Fig. S7). PCN-223 also manifests a small porphyrin-porphyrin torsional angle (~55^{o}) that facilitates interchromophoric electronic coupling between TCPP units.[13] Based on these merits, PCN-223 qualifies to serve as a model system to explore EET mechanism in porphyrin-based MOFs.

Herein, we present synthesis, structural, and photophysical characterization of PCN-223 MOF constructed from free base TCPP ligand. The effects of pH and temperature on the excited state properties of PCN-223(fb) were investigated and compared with those of ligand. The variable temperature measurements revealed the incoherent nature of excitation energy transfer (EET) in PCN-223. The excitation energy transfer was investigated by studying the pH dependence of photoluminescence (PL) quenching. The study revealed the presence of static quenching both in ligand and in MOF. Additionally, the study revealed that the PL quenching was greatly enhanced in MOF as compared to free ligand, and the efficiency of quenching increased from 51% in ligand to 93% in MOF. Förster energy transfer model was used to estimate the rate of exciton hopping (k_{hop}) and the exciton hopping time in PCN-223. Nanosecond transient absorption spectroscopy was used to characterize the nature of non-emissive triplet state. The study revealed the presence of a long-lived triplet state extending beyond 200 µs and having the signature characteristic feature of a TCPP based triplet state. Femtosecond transient absorption spectroscopy was employed to characterize the ultrafast processes taking place in TCPP and PCN-223. Kinetic analysis of the ultrafast data of TCPP and PCN-223 revealed the presence of three distinct time components that correspond to: (a) solvent-induced vibrational reorganization of excitation energy, (b) vibrational cooling, and (c) fluorescence. Our study revealed the presence of efficient excitation energy transfer and long-distance exciton hopping (100 Å (1D), 141 Å (2D), and 173 Å (3D)) in PCN-223 MOF.

Experimental section

Materials: Meso-tetracarboxyphenylporphyrin (>97%) was purchased from Frontier Scientific and was used without further purification. Zirconium chloride (anhydrous, ≥99.5%) was purchased from Sigma-Aldrich. Dimethylformamide (DMF, spectrophotometric grade, ≥99.9%) was purchased from Fisher chemical. Propionic acid (PA, 99%). were purchased from Alfa Aesar.

Synthesis of PCN-223(fb): 10 mg of H_2TCPP (1.3×10^{-5} moles) and 7 mg of $ZrCl_4$ (3×10^{-5} moles) were added to 10ml DMF and ultrasonically dissolved in a 6-dram vial. 2 ml propionic acid was added to the vial and the vial was sonicated for 15 minutes to get a homogeneous reaction mixture. The vial was placed in an oven set at 120 ^{o}C for 16 hours. After allowing them to cool down to room temperature, the resultant MOF powder was collected by centrifugation. It was washed 3 times with DMF and then soaked in ethanol for 3 days with fresh ethanol replacement every day. The MOFs were dried at room temperature and then activated by heating at 100 °C under vacuum.

Powder X-ray diffraction and Scanning electron microscopy (PXRD): A 600 W Rigaku MiniFlex powder diffractometer with a CuKα (0.15418 nm) radiation source was used, with a sweeping range of 2–25° in continuous scanning mode. PXRD traces were collected in 0.05° increments at a scanning rate of 0.2°/min.

Scanning electron microscopy (SEM): SEM samples were prepared by suspending MOF powders in ethanol with sonication. The resulting suspensions were drop-casted on precut glass slides. After drying, the glass slides were mounted on SEM sample pegs with the help of double-sided copper tape. The sides of the glass slides and the platform of sample peg were coated with conductive carbon paint purchased from Electron Microscopy Sciences. A LEO (Zeiss) 1550 field-emission scanning electron microscope, equipped with an in-lens detector, operating at 5.0 kV was used to obtain high-resolution images of the MOF particles.

Thermogravimetric Analysis (TGA): A Q-series thermogravimetric analyzer from TA Instruments was used to assess the thermal stability of MOFs. Samples weighing ~3-5 mg were placed on a platinum pan and heated under air at a rate of 5 °C/min over the temperature range of 25−800 °C.

Gas Sorption Isotherms: The N_2 adsorption measurements were conducted using a Micromeritics 3Flex instrument. A 6 mm large bulb sample cell was used to hold the samples and was degassed under vacuum at a temperature of 100 °C for 24 h. The surface area of the MOFs was determined from the N_2 adsorption isotherms at 77 K by fitting the adsorption data within the 0.05−0.3 P/P_0 pressure range to the BET equation.

Diffuse absorption spectroscopy: The diffuse absorption spectra of TCPP and PCN-223(fb) were obtained using an Agilent Technologies 8453 UV-Vis diode array spectrophotometer (1 nm resolution) where the sample compartment was replaced with an integration sphere. The powder samples were diluted by mixing with $BaSO_4$.

Steady-state emission spectroscopy and time-resolved emission lifetimes: The steady-state emission spectra were obtained using a QuantaMaster Model QM-200-4E emission spectrophotometer from Photon Technology, Inc. (PTI). The excitation light source was a 75 W Xe arc lamp (Newport). The detector was a thermoelectrically cooled Hamamatsu 1527 photomultiplier tube (PMT). Emission traces were analyzed using Origin 9.0. Time-resolved fluorescence lifetimes were obtained via the time-correlated single photon counting technique (TCSPC) with the same QuantaMaster Model QM-200-4E emission spectrophotometer from Photon Technology, Inc. (PTI) equipped with a 415 nm LED and a Becker & Hickl GmbH PMH-100 PMT detector with time resolution of < 220 ps FWHM. Florescence lifetime decays were analyzed with the help of Origin 9.0.

Nanosecond transient absorption spectroscopy:

Transient absorption difference spectra and kinetic traces were collected with LP 980 laser flash photolysis system (Edinburgh Instruments) equipped with a PMT detector (R928, Hamamatsu). The excitation source was 532 nm Nd:YAG laser (Spectra-Physics-Quanta-Ray Lab) operating at 1 Hz. The laser

system was also equipped with an image intensified CCD (ICCD) camera detector. Triplet lifetime decays were analyzed with the help of Origin 9.0.

Femtosecond transient absorption spectroscopy:

Time-resolved transient absorption measurements were performed at the Imaging and Kinetic Spectroscopy (IMAKS) Laboratory, Department of Chemistry, NCSU (North Carolina State University). A mode-locked Ti:sapphire laser (Coherent Libra, 800 nm, 1 kHz repetition rate, 100 fs, 4 mJ/pulse) was used as the main light source. The output from the laser was split into the pump beam and probe beam. The pump beam was directed into the parametric amplifier (Coherent OPerA Solo) to generate the 400nm excitation. The probe beam was delayed in a 6ns optical delay stage and then focused into a CaF_2 crystal for white light continuum generation between 340 nm and 750 nm. The pump beam was then focused on the sample (into an 800 μm spot) and overlapped with the probe beam (~200 μm). The relative polarizations of the pump beam and the probe beam were set at the magic angle of 54.7º. The ground state absorption spectra of the samples were measured before and after the measurements to ensure that there is no degradation. Transient kinetics were analyzed using the fitting routines available in Origin 9.0.

Results and Discussion

Synthesis of PCN-223(fb) was achieved by following a procedure that gives highly crystalline, phase-pure powder. Briefly, 3×10^{-5} moles of $ZrCl_4$ and 1.3×10^{-5} moles of TCPP were dissolved in 10 mL DMF along with 2.5×10^{-2} moles of propionic acid as the modulator. The mixture was sonicated for 15 minutes then the vial was placed in an oven and heated at 120 ºC for 16 h. PCN-223(fb) MOF powders were characterized by PXRD (Fig. 2a) and SEM (Fig. 2b). Comparison of the PXRD pattern obtained from synthesis to the simulated pattern from single crystal XRD data indicated high phase purity. SEM image shows small bean-shaped particles that are characteristic of PCN-223 MOF. All MOF particles are morphologically identical, which further verifies the phase purity. In addition, thermal stability and surface area of as-prepared PCN-223(fb) were studied with the help of thermogravimetric analysis and N_2 adsorption isotherm. The BET surface area of the MOF obtained from the gas adsorption data agrees well with literature (see supporting information, Fig. S1 and S2).[10]

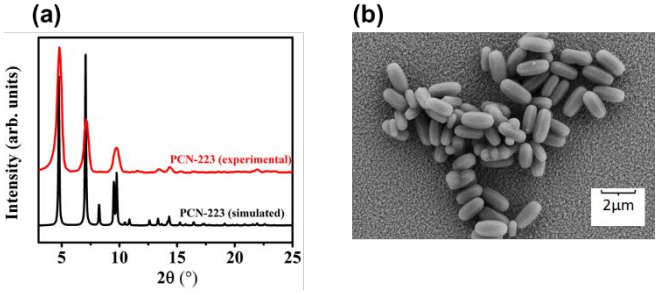

Figure 2. (a) PXRD characterization of PCN-223(fb) (b) SEM image of PCN-223(fb)

To examine how the ground and excited-state properties of TCPP are affected upon coordination into the MOF structure, the absorption spectra of TCPP and PCN-223(fb) were compared (Fig. 3). The electronic absorption spectrum of TCPP consists of two distinct regions. The first involves the transition from the ground state to the second excited state ($S_0 \rightarrow S_2$) and the corresponding band is called the Soret or B band. The second region consists of a weak transition to the first excited state ($S_0 \rightarrow S_1$) in the range of 500-750 nm (the Q bands). PCN-223(fb) displays an absorption spectrum similar to that of TCPP with a sharp Soret band and four Q bands. The Soret band of PCN-223 is blue shifted by 13 nm relative to the ligand, which is attributed to structural changes that TCPP undergoes as it is incorporated in the MOF. Twisting of phenyl rings and changes in the macrocyclic ring planarity of TCPP may be responsible for increasing the electronic transition energy-gap (S_0-S_2), which causes the blue shift. The peak positions and the peak intensities of Q bands of PCN-223 match those of TCPP (see supporting information, Table 1), suggesting that the energy gap between ground state and first excited state of TCPP is relatively unaffected upon incorporation in MOF.

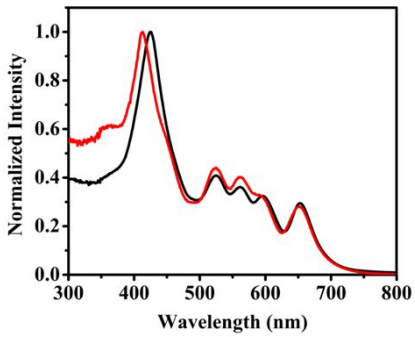

Figure 3. Diffuse absorption spectra of TCPP (black) and PCN-223(fb) (red)

The acid-base properties of porphyrins in aqueous solutions provide important information about their reactivity, aromaticity, tautomerization mechanisms and stereochemistry.[14–16] The central macrocycle of porphyrins exhibits an amphoteric behavior and can exist in either neutral (free-base), N-protonated, or deprotonated form (Fig. 4). Mono-protonation of the free-base form induces nonplanar distortions in the porphyrin structure, which makes the second protonation more favorable.[17,18] The first protonation step is immediately followed by the second step, producing the porphyrin dication, while the monoprotonated species is present in very small amounts at any given time. To determine the pK_a values corresponding to the successive protonation steps, TCPP solution (10^{-6} M) and MOF suspension in water were titrated against 0.01 M NaOH solution (see supporting information, Fig. S3 and S4). The pK_a values are reported in Fig.4.

Varying solution pH can shift the protonation-deprotonation equilibrium of the macrocycle in favour of a particular form,

which has been shown to greatly influence the photophysics of the porphyrin molecule.[18] Non-planarity induced in the porphyrin structure due to protonation of the nitrogen atoms breaks up their π-electron conjugated double-bond system. Loss of conjugation promotes non-radiative relaxation of excited state that results in significant fluorescence quenching and short fluorescence lifetimes.[19] To investigate the effects of pH variation on the fluorescence properties of TCPP and PCN-223(fb), their steady-state emission spectra were measured in an experimental pH range of 3.5 to 8.5 ($\lambda_{excitation}$ = 415 nm). Given that PCN-223(fb) is stable in aqueous environments with pH values ranging from 0 to 10,[10] the experimental pH range is suitable for investigating the photophysics of the MOF without loss in crystallinity. The peak positions and intensities of fluorescence spectra of TCPP and PCN-223(fb) were found to be strongly correlated with pH of solution/suspension. The fluorescence spectra of the neutral form of TCPP and PCN-223(fb) (5.5 < pH < 8.5) displayed a sharp band at 645 nm (Q(0,0)) and a relatively weaker band at 720 nm (Q(0,1)) (Fig 5a and 5b). Structural changes induced in the porphyrin macrocycle due to protonation of central nitrogen atoms cause the band at 645 nm to broaden and red shift by ~35 nm. As a result, the fluorescence spectrum appears to be a single broad band with a maximum at 680 nm (Fig. 5c).

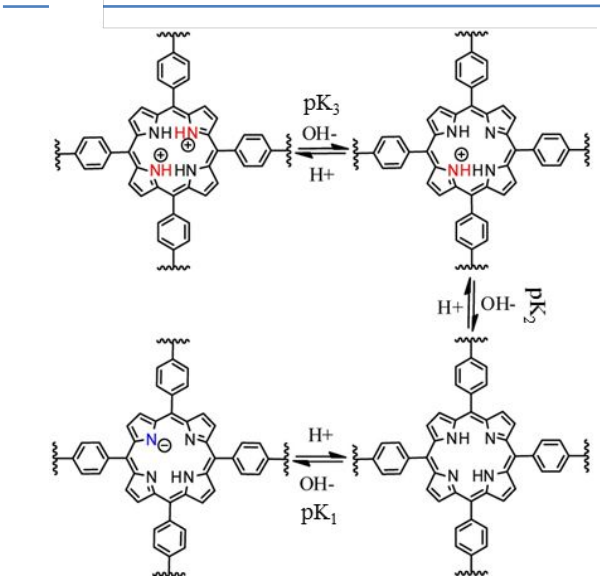

Figure 4. Protonation and deprotonation processes of TCPP in acidic and basic media.[8] pK_1, pK_2 and pK_3 represent the pK_a values associated with these processes. The first and second protonation processes are almost indistinguishable, such that $pK_2 \approx pK_3$. For TCPP, $pK_2 \approx pK_3$ = 3.2, and for PCN-223 $pK_2 \approx pK_3$ = 3.75 (see supporting information, Fig. S3 and S4).

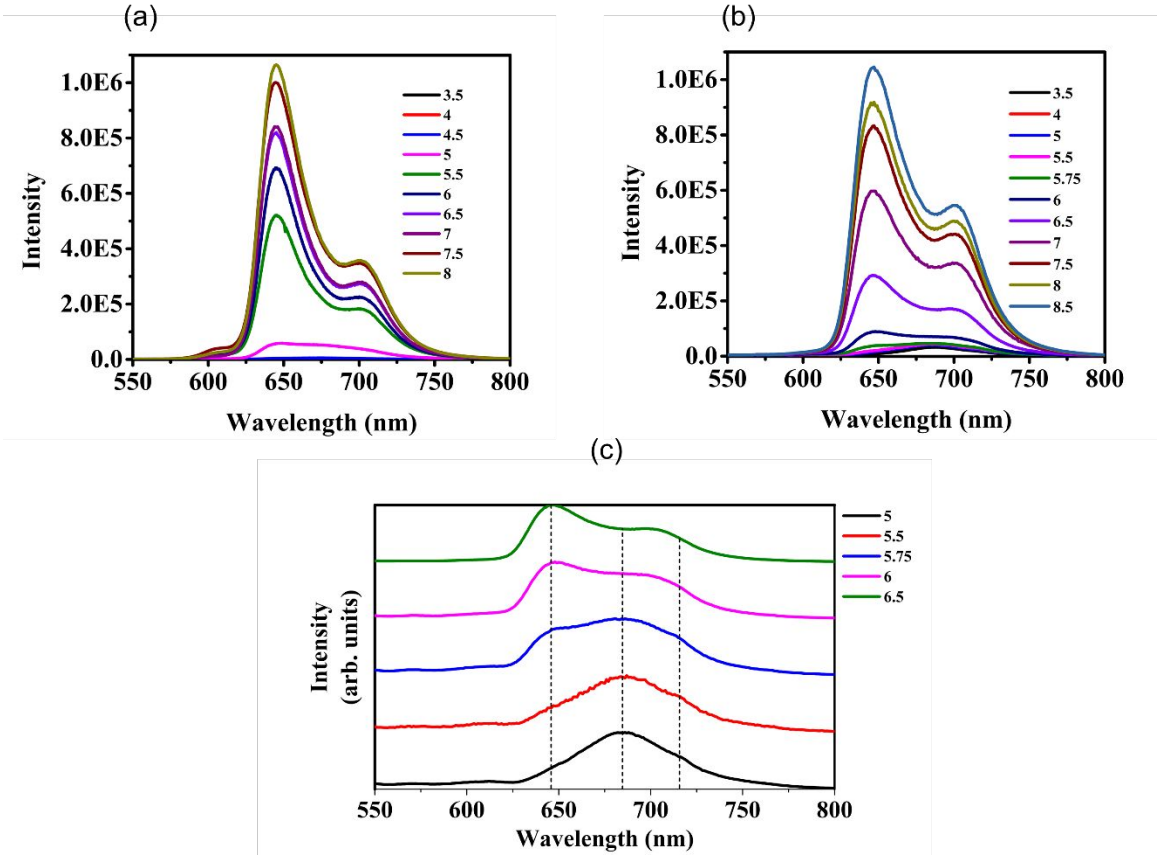

Figure 5. (a) Fluorescence spectra of TCPP in water (10^{-6}M) as a function of pH (b) Fluorescence spectra of PCN-223(fb) in water as a function of pH. (c) Spectral evolution of PCN-223(fb) in pH range of 5 to 6.5.

Temperature dependence of fluorescence lifetimes

Temperature dependence of the fluorescence decay rates (k_{obs}) of an emissive MOF can give insight into the mechanism of energy transfer.[20] At room temperature, there are various vibrational degrees of freedom that allow the excited state to fully relax between energy transfer events. However, at low temperatures (~77K) some of the vibrational degrees of freedom are frozen out. If the electronic interactions between the linkers in a MOF are very strong (strong coupling regime), then at low temperatures the rate of energy transfer can exceed that of vibrational relaxation. In such a scenario, the excitation energy can move as an exciton that is delocalized over the whole system.[1,21] The MOF should behave as an "aggregate" and the energy transfer process is termed as "coherent". In contrast, if the electronic interactions between the linkers in a MOF are weak (weak coupling regime), then vibrational relaxation dominates at all temperatures. At a given time "t", the excitation energy remains localized on a linker. The MOF behaves as a "monomer" and the excitation energy transfer is termed as "incoherent".

To determine whether PCN-223(fb) belongs to the strong coupling regime or the weak coupling regime, the temperature-dependent fluorescence decay kinetics of TCPP and PCN-223(fb) were compared.[22] The fluorescence decay rates of TCPP and PCN-223(fb) were obtained at temperatures ranging from 77K to 333K (Fig. 6a and 6b). To plot the temperature dependence curves, the experimental decay rates were fit to the following equation-

$$k_{obs} = k_0 + k_1 e^{-\Delta E/k_B T}$$

where k_0 is the temperature independent term and the Arrhenius term describes the temperature dependence of k_{obs}.[23,24] The parameters extracted from the fits are reported in Table 1. The pre-exponential factor or the frequency factor (k_1) and the activation energy for transitioning from the ground state to the excited state (ΔE) of TCPP and PCN-223(fb) are very similar, suggesting that the temperature-dependent fluorescence behavior of the MOF is comparable to that of monomer TCPP units. This result implies that PCN-223(fb) belongs to the weak coupling regime. Therefore, we propose an incoherent mechanism for EET in PCN-223(fb) MOF.

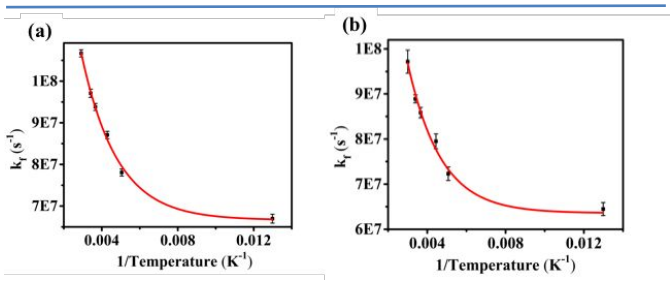

Figure 6.(a) Temperature dependence of the observed emission decay rates of TCPP in MeOH-EtOH (3:1 v/v) mixture (pH ≈ 7) (b) Temperature dependence of the observed emission decay rates of PCN-223(fb) suspension (3:1 v/v) mixture (pH ≈ 7).

Table 1. Experimental parameters associated with TCPP and PCN-223(fb)

	k_0 (s^{-1}) ($\times 10^7$)	k_1 (s^{-1}) ($\times 10^7$)	ΔE (J/molecule) ($\times 10^{-21}$)
TCPP	6.7 ± 0.1	4 ± 0.1	7.3 ± 0.1
PCN-223	6.4 ± 0.2	3.3 ± 0.6	8.3 ± 0.5

Photoluminescence quenching

The energy transfer efficiency of porphyrin-based MOFs can be evaluated by relating the concentration of quencher to the extent of photoluminescence quenching.[25,26] Typically, quenching experiments on MOF are carried out in the presence of an external quencher on its surface. The pH-dependence of the fluorescence intensity in PCN-223 MOF shows that N-protonated porphyrins can potentially act as an internal quencher. Due to the presence of this internal quenching, no additional quencher was used in this study. The relationship between the quencher concentration and extent of quenching is provided by Stern-Volmer equation,

$$I_0/I = 1 + K_{SV}[Q]$$

where I_0 is the fluorescence intensity in the absence of quencher, I is the fluorescence intensity at a particular concentration of quencher, K_{SV} is the Stern-Volmer quenching constant, and [Q] is the quencher concentration. Fig. 7 shows the modified Stern-Volmer plot for TCPP and PCN-223, where I_0/I is plotted against that ratio of N-protonated and neutral ligand concentration (see supporting information, section 5).

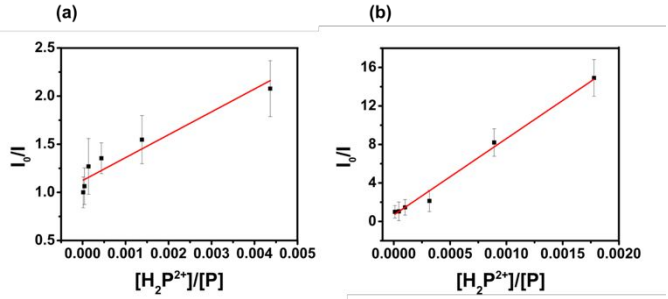

Figure 7. (**a**) Modified Stern-Volmer plot of TCPP in the pH range of 5.5 to 8.5 (**b**) Modified Stern-Volmer plot of PCN-223(fb) in the pH range of 5.5 to 8.5.

Table 2. Stern-Volmer rate constant and quenching rate constants of TCPP and PCN-223(fb)

	K_{sv} (M^{-1})	k_Q ($M^{-1}s^{-1}$)
TCPP	237.68	2.71×10^{10}
PCN-223(fb)	7298.96	8.06×10^{11}

The quenching rate k_Q can be calculated by dividing K_{SV} with the fluorescence lifetime of donor in the absence of quencher (τ_0). The Stern-Volmer rate constants and quenching rate constants of TCPP and PCN-223(fb) are provided in Table 2. The quenching rate in PCN-223 is relatively higher than TCPP (by an order of

10), which is attributed to energy migration from neutral TCPP units to N-protonated ones. Although a dramatic decrease in photoluminescence intensity of MOF was observed on lowering the pH, time resolved photoluminescence decay measurements revealed that the lifetime of the MOF was not quenched.

Energy transfer efficiency in PCN-223(fb)

Excitation energy transfer primarily occurs through two coupling mechanisms: Dexter exchange mechanism and Förster dipole-dipole mechanism.[4,26–30] The Dexter mechanism requires the presence of electronic communication between the donor and acceptor via orbital overlap.[31,32] Since the orbital overlap between adjacent porphyrin struts in Zr-based MOFs with porphyrin linkers is poor, the Dexter mechanism may not be suitable to describe energy transfer in these MOFs.[20] The Förster mechanism (FRET), on the other hand, adequately describes the "through space" energy migration in these MOFs. The rate and efficiency of FRET is dependent on three physical parameters. These parameters are (1) the degree of overlap between donor emission and acceptor absorption (spectral overlap, *J*), (2) the relative geometric orientation of donor and acceptor within the framework, (3) the distance between the donor and acceptor in the framework.[33] The FRET efficiency of porphyrin-based MOFs has been previously quantified by performing photoluminescence quenching experiments.[20,28,34] A qualitative analysis of FRET efficiency was performed by relating the extent of quenching (Φ_q) to the concentration of quencher (N-protonated porphyrin). Φ_q is defined as,

$$\Phi_q = 1 - I_q/I_0$$

where I_q and I_0 are the PL intensities of donor in the presence and absence of quencher.[35] The concentration of N-protonated TCPP in solution and MOF at a given pH can be found using the Henderson-Hasselbalch equation. The concentration of N-protonated TCPP in solution and MOF is ~1% at pH 5.5 and 6 respectively. The emission intensity of monomeric TCPP solution and MOF at pH 5.5 and 6 was set as I_q. The emission intensity at pH 8 was set as I_0. The Φ_q for TCPP and PCN-223 was estimated to be 93% and 51% respectively. The significantly higher magnitude of Φ_q in MOF complements the results of PL quenching in the previous section. The quenching observed in MOF can be considered as a combination of "self-quenching" and quenching via energy transfer from neutral porphyrins to N-protonated porphyrins.

The rate of energy transfer defined by Förster model is given by,

$$k_{ET} = \frac{1}{\tau_0}\left(\frac{R_0}{r}\right)^6$$

where τ_0 is the lifetime of donor in the absence of acceptor, r is the donor-acceptor distance and R_0 is the Förster radius.[21] R_0 is defined as the distance at which the energy transfer efficiency is 50%, and is dependent on the fluorescence quantum yield of donor in the absence of acceptor (Φ_D) and the overlap integral (J).

$$R_0 = \left(\frac{9000(\ln 10)K^2\Phi_D J}{128\pi^5 N_A \eta^4}\right)^{1/6}$$

where κ^2 is a geometric parameter that describes the relative orientation between the transition dipole moments of donor and acceptor, N_A is Avogadro's number, and n is the refractive index of the surrounding media. Based on the above equation, the Förster radius for PCN-223 was found to be 54.5 Å (J = 5.344 $\times$ 10^{-14} $M^{-1}cm^3$, see supporting information, Fig. S6). Quantum yield was obtained by relative method (0.27) (see supporting information, section 8). Quantum yield of TCPP in methanol was obtained from literature.[36] The spectral overlap integral of TCPP previously reported in literature is 2.49 $\times$ 10^{-15} $M^{-1}cm^3$.[37] The rate of exciton hopping (k_{hop}) and exciton hopping time were estimated to be 1.9 $\times$ 10^{12} s^{-1} and 0.53 ps respectively. These values are broadly consistent with those reported by Son et. al. for other porphyrin-based MOFs.[25] The total exciton hopping distance was obtained from,

$$R_{hop} = \sqrt{m\frac{D_m}{R_0}}$$

where D_m is the exciton diffusion coefficient.[36–40] Long distance exciton hopping corresponding to 100 Å for one-dimensional energy transfer, 141 Å for two-dimensional energy transfer, and 173 Å for three-dimensional energy transfer was estimated. Since there is limited information about the singlet exciton diffusion coefficient of porphyrin-based MOFs, the exciton diffusion coefficient of TPPS nanotubes (95 $\times$ 10^{-6} m^2 s^{-1}) was used for the calculation of exciton hopping distance.[36]

Nanosecond transient absorption spectroscopy

Thus far, we have investigated the singlet excited states of TCPP and PCN-223(fb). Nanosecond transient absorption (nsTA) spectroscopy was used as an additional tool to get further insight into the excited state photophysics of TCPP and PCN-223(fb). With the help of this technique, the triplet excited state of TCPP and PCN-223(fb) were studied. Nanosecond transient absorption difference spectra were acquired for TCPP solution and PCN-223(fb) suspension in water at pH 8 (in the nanosecond to microsecond time domain, Fig 8a and 8b). The resulting difference spectra for both TCPP and PCN-223(fb) were almost identical, having an intense ground state bleach at ~420 nm followed by an excited state absorption band centred near 470 nm. The study also revealed that the nature of excited state did not change between nanosecond to microsecond time domain (see supporting information, Fig. S8). The transient absorption decay of TCPP at 470 nm exhibited single-exponential kinetics with a lifetime of 260 $\pm$ 7 µs (Fig. 8c). The triplet lifetime of TCPP was in good agreement with the previously reported studies.[41] PCN-223(fb) also exhibited a mono-exponential decay with a lifetime of 201 $\pm$ 27 µs (Fig. 8d). Due to the rigidity of the MOF structure, the rate of non-radiative deactivation pathways is expected to decrease, which in turn should lead to an increase in the lifetime of TCPP incorporated in PCN-223(fb). Contrastingly, the lifetime of PCN-223(fb) was found to be relatively shorter as compared to the ligand. The shorter triplet lifetime of PCN-223(fb) may be attributed to energy transfer pathways within the donor-

acceptor framework. One of the possible pathways could potentially be energy transfer to the trap states such as N-protonated porphyrins and structural defects in MOF. In order to further investigate the role of N-protonated porphyrins as quenchers, nanosecond transient absorption measurements were attempted at different pH values. However, the solubility of TCPP in water dramatically decreases on lowering the pH, resulting in very weak transient signal. Consequently, nsTA measurements were not successful at low pH.

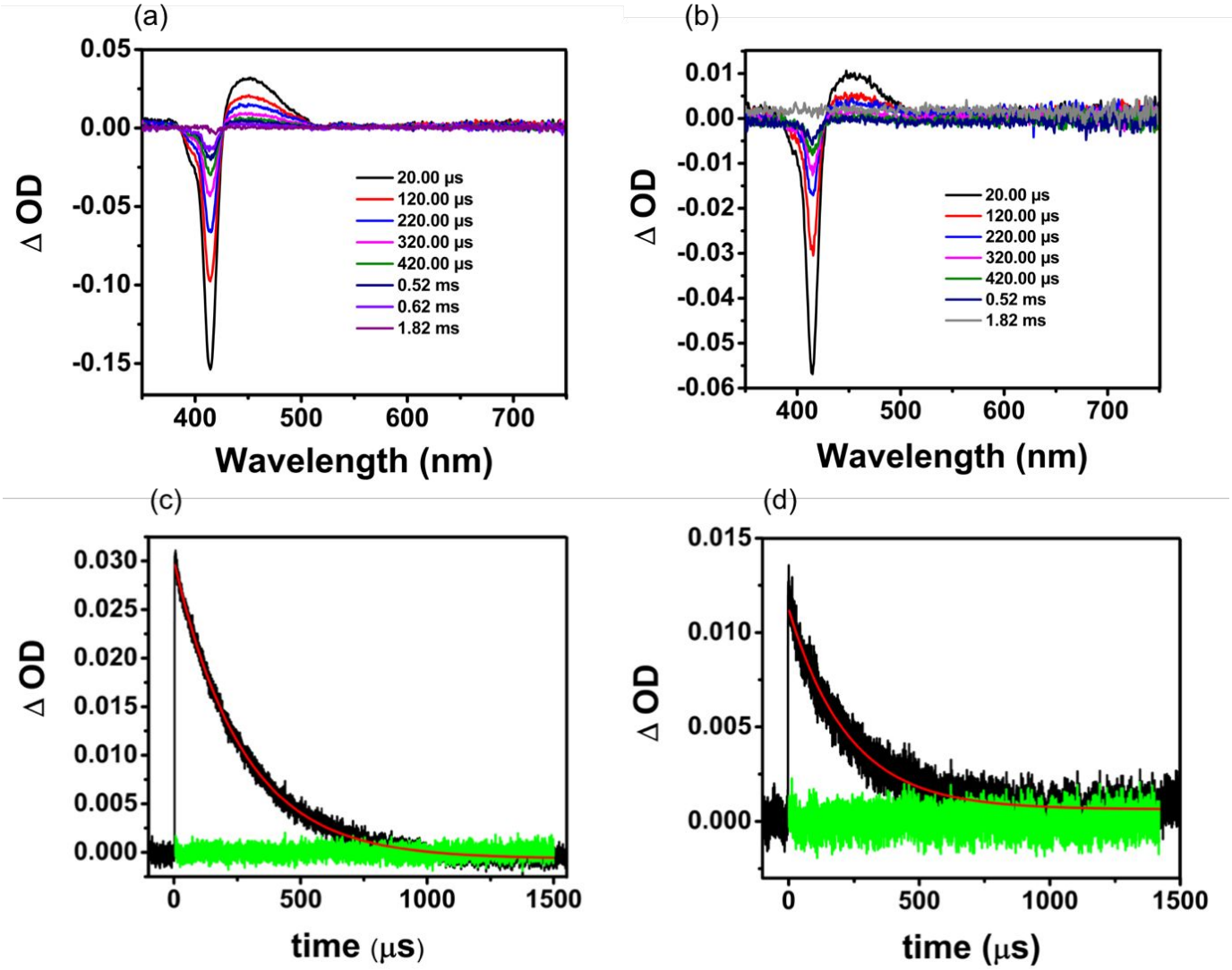

Figure 8. Transient absorption difference spectra (mapping) of (a) TCPP and (b) PCN-223(fb) measured in degassed water at room temperature following 532 nm pulsed laser excitation (4-5 mJ/pulse, 5−7 ns fwhm). Both difference spectra represent an average of 30 transients. Fitted transient absorption decay of (c) TCPP and (d) PCN-223(fb) along with the residuals (green coloured). Both the transient absorption kinetic measurements were probed at 470 nm.

Femtosecond Transient absorption spectroscopy

To further map the excited state trajectory across all available timescales, ultrafast transient absorption (fsTA) studies on TCPP and PCN-223 were performed with 400 nm excitation and probe wavelengths that ranged across the UV-Visible region. The fsTA difference spectra of both TCPP and PCN-223(fb) consists of a ground state bleach at 415 nm followed by an excited state absorption band starting from 430 nm. Composite spectral features that can be attributed to ground state bleach (from the Q band absorption) and excited state absorption can be observed in the 500-650 nm range. The evolution of their transients is presented in Fig. 9a and 9b. Over the course of the first 500 fs, the ground state bleach at 415 nm and the excited state absorbance centred near 470 nm appear. As time progresses, no change is observed in the positions of the bands. The features in the fsTA difference spectrum of TCPP and PCN-223 qualitatively match those of the nsTA difference spectrum (see supporting information, Fig. S9a and S9b), signifying that the nature of excited state in both the ligand and the MOF did not change as we moved from the femtosecond to microsecond time domain.

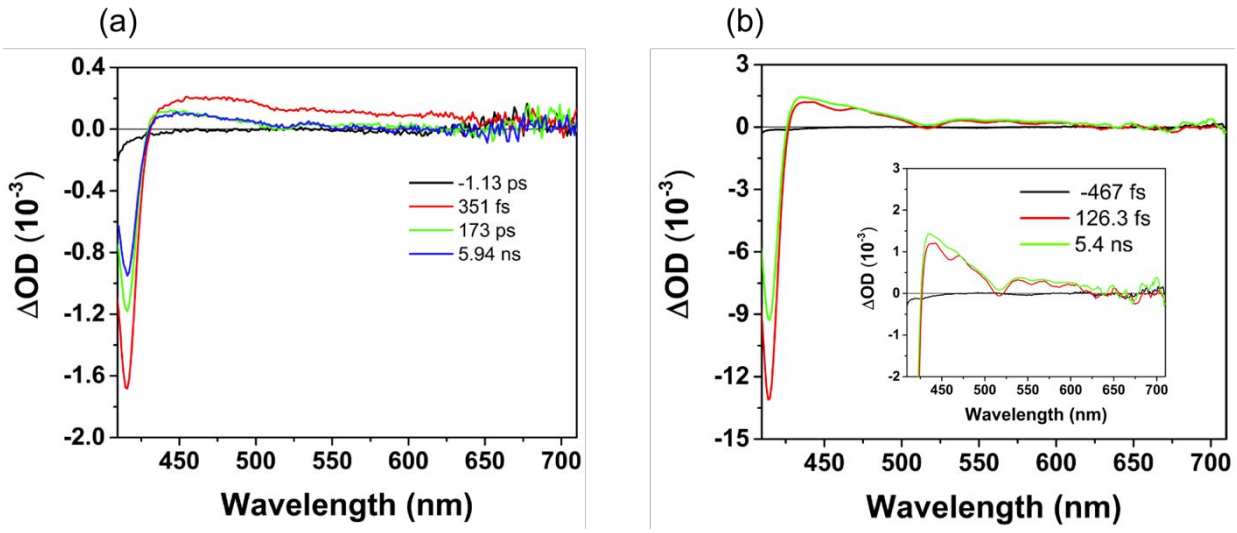

Figure 9. Transient absorption difference spectra of (a)TCPP (in a 1:1 (v/v) water-ethanol mixture (~ 10^{-6} M)) at pH-8 following 400 nm pulsed laser excitation (140 fs fwhm), (b) PCN-223 in water at pH-8 following 400 nm pulsed laser excitation (140 fs fwhm). Inset shows an expanded view of the excited state absorption band. Experimental delay times are indicated in the legend.

The transient kinetics of TCPP were probed at 418 nm and 506 nm, and analysed using single and multiexponential models (see supporting information, Fig. S10(a)). The kinetic trace at 418 nm was best fit to a triexponential model. The lifetimes determined from the fit are provided in Table 3. Following previous assignments provided in the literature,[42–47] the shortest component (τ_1) is assigned to a solvent-induced process that causes vibrational reorganization of excitation energy in S_1 state of TCPP (solvent reorganization). Elastic collisions between the ligand and solvent molecules are believed to be responsible for this process. The second component (τ_2) is attributed to vibrational relaxation of excited state S_1 due to interaction with solvent molecules (vibrational cooling). The third component is too long to be measured accurately with our apparatus and is attributed to fluorescence in TCPP.[42] The trace at 506 nm exhibited single exponential decay kinetics with a lifetime consistent with the vibrational cooling component of excited state relaxation.

In the case of PCN-223 MOF, the kinetics were probed at 348 nm and 510 nm (see supporting information, Fig. S10(b)). Kinetic analysis of the ultrafast data revealed the presence of three distinct time constants (Table 4). Based on a comparison between the time constants of TCPP and PCN-223, the first component (τ_1) is assigned to solvent reorganization. The second component (τ_2) is assigned to vibrational cooling in MOF. The third component ($\tau_3 > 1$ns) is assigned to fluorescence in MOF.

It is worth noting that the lifetime corresponding to solvent reorganization and vibrational cooling in MOF is relatively higher as compared to the free ligand. Such an observation can be explained by three potential hypotheses. The first is that immobilization of the TCPP within the 3D rigid structure of MOF decreases the vibrational modes able to couple to this cooling process. Similar observations have been observed, i.e. the decrease in non-radiative, vibrational excited state decay, in chromophore modified MOFs.[48,49] The second is that the solvent molecules coupled to the vibrational cooling process have less accessibility to the porphyrin units in the MOF. The third hypothesis attributes the observed differences in the lifetimes between the TCPP and MOF samples to the different solvent systems used to measure each. Ultrafast TA measurements on TCPP samples were conducted in a 1:1 (v/v) mixture of water and ethanol. Ethanol was added to improve the solubility of TCPP in water, which in turn improves its absorbance. On the other hand, fsTA measurements on MOF samples were conducted in water (without ethanol). The difference in solvent polarities may be responsible for the higher lifetimes in MOF.

Table 3. Time constants obtained for TCPP in 1:1 water-ethanol mixture at selected probe wavelengths (pump wavelength = 400 nm)

Wavelength (nm)	τ_1	τ_2	τ_3
418 nm	2 ± 1 ps	57 ± 22 ps	>1 ns
506 nm	51 ± 26 ps	-	-

Table 4. Time constants obtained for PCN-223 in water at selected probe wavelengths (pump wavelength = 400 nm)

Wavelength (nm)	τ_1	τ_2	τ_3
348 nm	5 ± 2 ps	115 ± 22 ps	>1 ns
510 nm	123 ± 29 ps	-	-

Conclusions

In summary, PCN-223 MOF was synthesized from free base TCPP and was thoroughly characterized. The photophysical properties of the synthesized MOF and the free ligand were explored extensively with various steady state and time-resolved spectroscopic techniques. The pH dependence of the fluorescence intensity of TCPP and PCN-223(fb) was investigated. Temperature dependence of the observed

fluorescence decay rates of PCN-223(fb) was comparable to that of monomeric TCPP units, suggesting that the interchromophoric interactions between TCPP linkers in MOF belong to the weak coupling regime. Therefore, an incoherent, hopping type mechanism was proposed for EET in PCN-223(fb). Internal fluorescence quenching experiments demonstrate that the singlet-state of PCN-223(fb) (in suspension) is quenched to a greater extent than ligand (in solution). PCN-223(fb) demonstrated a significantly higher extent of quenching (Φ_q = 93%) as compared to monomeric TCPP solution (Φ_q = 51%), at similar concentrations of quencher. The enhanced quenching in MOF is attributed to energy transfer from the freebase porphyrin linkers to N-protonated porphyrin linkers. The rate of exciton hopping and exciton hopping time in PCN-223 were estimated by using the Förster energy transfer model. These values were found to be consistent with other porphyrin-based MOFs. Femtosecond and nanosecond transient absorption studies were conducted on free ligand and MOF to characterize their excited state properties. Nanosecond transient absorption decays showed that the triplet lifetime of MOF is relatively shorter than the ligand, which may be due to triplet-triplet energy transfer to N-protonated porphyrins. Structural defects may also act as trap states and quench the triplet excited state of MOF. The enhanced exciton migration distance (173 Å in 3D) in PCN-223(fb) MOF suggests that this type of chromophoric system could potentially have useful application as light-harvesters in various solar energy conversion devices.

Conflicts of interest

The authors declare no conflicts of interest in preparation of this article.

Acknowledgements

This material is based upon work supported by the Department of Energy under Grant DE-SC0012445.

Notes and references

(1) Renger, T. *Photosynth. Res.* **2009**, *102* (2), 471–485.
(2) Yang, J.; Yoon, M.-C.; Yoo, H.; Kim, P.; Kim, D. *Chem. Soc. Rev.* **2012**, *41* (14), 4808–4826.
(3) Li, Y.; Xu, H.; Ouyang, S.; Ye, J. *Phys. Chem. Chem. Phys.* **2016**, *18* (11), 7563–7572.
(4) So, M. C.; Wiederrecht, G. P.; Mondloch, J. E.; Hupp, J. T.; Farha, O. K. *Chem. Commun.* **2015**, *51* (17), 3501–3510.
(5) Furukawa, H.; Cordova, K. E.; O'Keeffe, M.; Yaghi, O. M. *Science (80-.).* **2013**, *341* (August), 974.
(6) Kuc, A.; Enyashin, A.; Seifert, G. *J. Phys. Chem. B* **2007**, *111* (28), 8179–8186.
(7) Feng, D.; Gu, Z.-Y.; Li, J.-R.; Jiang, H.-L.; Wei, Z.; Zhou, H.-C. *Angew. Chemie Int. Ed.* **2012**, *51* (41), 10307–10310.
(8) Jiang, H.-L.; Feng, D.; Wang, K.; Gu, Z.-Y.; Wei, Z.; Chen, Y.-P.; Zhou, H.-C. *J. Am. Chem. Soc.* **2013**, *135* (37), 13934–13938.
(9) Morris, W.; Volosskiy, B.; Demir, S.; Gándara, F.; McGrier, P. L.; Furukawa, H.; Cascio, D.; Stoddart, J. F.; Yaghi, O. M. *Inorg. Chem.* **2012**, *51* (12), 6443–6445.
(10) Feng, D.; Gu, Z.-Y.; Chen, Y.-P.; Park, J.; Wei, Z.; Sun, Y.; Bosch, M.; Yuan, S.; Zhou, H.-C. *J. Am. Chem. Soc.* **2014**, *136* (51), 17714–17717.
(11) Feng, D.; Jiang, H.-L.; Chen, Y.-P.; Gu, Z.-Y.; Wei, Z.; Zhou, H.-C. *Inorg. Chem.* **2013**, *52* (21), 12661–12667.
(12) Deria, P.; Gómez-Gualdrón, D. A.; Hod, I.; Snurr, R. Q.; Hupp, J. T.; Farha, O. K. *J. Am. Chem. Soc.* **2016**, *138* (43), 14449–14457.
(13) Deria, P.; Yu, J.; Balaraman, R. P.; Mashni, J.; White, S. N. *Chem. Commun.* **2016**, *52* (88), 13031–13034.
(14) Seybold, P. G.; Gouterman, M. *J. Mol. Spectrosc.* **1969**, *31* (1–13), 1–13.
(15) Biesaga, M.; Pyrzyńska, K.; Trojanowicz, M. *Talanta* **2000**, *51* (2), 209–224.
(16) Lo, P.-C.; Leng, X.; Ng, D. K. P. *Coord. Chem. Rev.* **2007**, *251* (17), 2334–2353.
(17) Rudine, A. B.; DelFatti, B. D.; Wamser, C. C. *J. Org. Chem.* **2013**, *78* (12), 6040–6049.
(18) Hynninen, P. H. *J. Chem. Soc. Perkin Trans. 2* **1991**, No. 5, 669–678.
(19) Kruk, M. M.; Starukhin, A. S.; Maes, W. *Macroheterocycles* **2011**, *4* (2), 69–79.
(20) Zhu, J.; Shaikh, S.; Mayhall, N. J.; Morris, A. J. In *Elaboration and Applications of Metal-Organic Frameworks*; Series on Chemistry, Energy and the Environment; WORLD SCIENTIFIC, 2017; Vol. Volume 2, pp 581–654.
(21) Valeur, B.; Berberan-Santos, M. N. *Excitation Energy Transfer*; 2012.
(22) De Rossi, U.; Dähne, S.; Gomez, U.; Port, H. *Chem. Phys. Lett.* **1998**, *287* (3), 395–402.
(23) Abrahamsson, M.; Becker, H.-C.; Hammarström, L.; Bonnefous, C.; Chamchoumis, C.; Thummel, R. P. *Inorg. Chem.* **2007**, *46* (24), 10354–10364.
(24) Abrahamsson, M.; Becker, H.-C.; Hammarström, L. *Dalt. Trans.* **2017**, *46* (39), 13314–13321.
(25) Son, H. J.; Jin, S.; Patwardhan, S.; Wezenberg, S. J.; Jeong, N. C.; So, M.; Wilmer, C. E.; Sarjeant, A. A.; Schatz, G. C.; Snurr, R. Q.; Farha, O. K.; Wiederrecht, G. P.; Hupp, J. T. *J. Am. Chem. Soc.* **2013**, *135* (2), 862–869.
(26) Patwardhan, S.; Jin, S.; Son, H.-J.; Schatz, G. C. *Mater. Res. Soc. Symp. Proc.* **2013**, *1539*, 22–27.
(27) Son, H.-J.; Jin, S.; Patwardhan, S.; Wezenberg, S. J.; Jeong, N. C.; So, M.; Wilmer, C. E.; Sarjeant, A. A.; Schatz, G. C.; Snurr, R. Q.; Farha, O. K.; Wiederrecht, G. P.; Hupp, J. T. *J. Am. Chem. Soc.* **2013**, *135* (2), 862–869.
(28) Lee, C. Y.; Farha, O. K.; Hong, B. J.; Sarjeant, A. A.; Nguyen, S. T.; Hupp, J. T. *J. Am. Chem. Soc.* **2011**, *133* (40), 15858–15861.
(29) Kent, C. A.; Mehl, B. P.; Ma, L.; Papanikolas, J. M.; Meyer, T. J.; Lin, W. *J. Am. Chem. Soc.* **2010**, *132* (37), 12767–12769.
(30) Zhang, Q.; Zhang, C.; Cao, L.; Wang, Z.; An, B.; Lin, Z.; Huang, R.; Zhang, Z.; Wang, C.; Lin, W. *J. Am. Chem. Soc.* **2016**, *138* (16), 5308–5315.
(31) Dexter, D. L. *J. Chem. Phys.* **1953**, *21* (5), 836.

(32) Lin, J.; Hu, X.; Zhang, P.; Van Rynbach, A.; Beratan, D. N.; Kent, C. A.; Mehl, B. P.; Papanikolas, J. M.; Meyer, T. J.; Lin, W.; Skourtis, S. S.; Constantinou, M. *J. Phys. Chem. C* **2013**, *117* (43), 22250–22259.

(33) Andrews, D. L. *Chem. Phys.* **1989**, *135* (2), 195–201.

(34) Maligaspe, E.; Kumpulainen, T.; Lemmetyinen, H.; Tkachenko, N. V.; Subbaiyan, N. K.; Zandler, M. E.; D'Souza, F. *J. Phys. Chem. A* **2010**, *114* (1), 268–277.

(35) Majoul I., Jia Y., D. R. *Practical Fluorescence Resonance Energy Transfer or Molecular Nanobioscopy of Living Cells*; Springer, Boston, MA, 2006.

(36) Kim, T.; Ham, S.; Lee, S. H.; Hong, Y.; Kim, D. *Nanoscale* **2018**, *10* (35), 16438–16446.

(37) Siebbeles, L. D. A.; Huijser, A.; Savenije, T. J. *J. Mater. Chem.* **2009**, *19* (34), 6067–6072.

(38) Maza, W. A.; Haring, A. J.; Ahrenholtz, S. R.; Epley, C. C.; Lin, S. Y.; Morris, A. J. *Chem. Sci.* **2016**, *7* (1), 719–727.

(39) Kaushal, M.; Ortiz, A. L.; Kassel, J. A.; Hall, N.; Lee, T. D.; Singh, G.; Walter, M. G. *J. Mater. Chem. C* **2016**, *4* (24), 5602–5609.

(40) Mikhnenko, O. V; Blom, P. W. M.; Nguyen, T.-Q. *Energy Environ. Sci.* **2015**, *8* (7), 1867–1888.

(41) Kathiravan, A.; Renganathan, R.; Anandan, S. *J. Colloid Interface Sci.* **2010**, *348* (2), 642–648.

(42) Baskin, J. S.; Yu, H.-Z.; Zewail, A. H. *J. Phys. Chem. A* **2002**, *106* (42), 9837–9844.

(43) Yu, H.-Z.; Baskin, J. S.; Zewail, A. H. *J. Phys. Chem. A* **2002**, *106* (42), 9845–9854.

(44) Kumble, R.; Palese, S.; Lin, V. S.-Y.; Therien, M. J.; Hochstrasser, R. M. *J. Am. Chem. Soc.* **1998**, *120* (44), 11489–11498.

(45) Li, X.; Gong, C.; Gurzadyan, G. G.; Gelin, M. F.; Liu, J.; Sun, L. *J. Phys. Chem. C* **2018**, *122* (1), 50–61.

(46) Sorgues, S.; Poisson, L.; Raffael, K.; Krim, L.; Soep, B.; Shafizadeh, N. *J. Chem. Phys.* **2006**, *124* (11), 114302.

(47) Rodriguez, J.; Kirmaier, C.; Holten, D. *J. Chem. Phys.* **1991**, *94* (9), 6020–6029.

(48) Maza, W. A.; Padilla, R.; Morris, A. J. *J. Am. Chem. Soc.* **2015**, *137* (25), 8161–8168.

(49) Maza, W. A.; Morris, A. J. *J. Phys. Chem. C* **2014**, *118* (17), 8803–8817.

TOC GRAPHIC

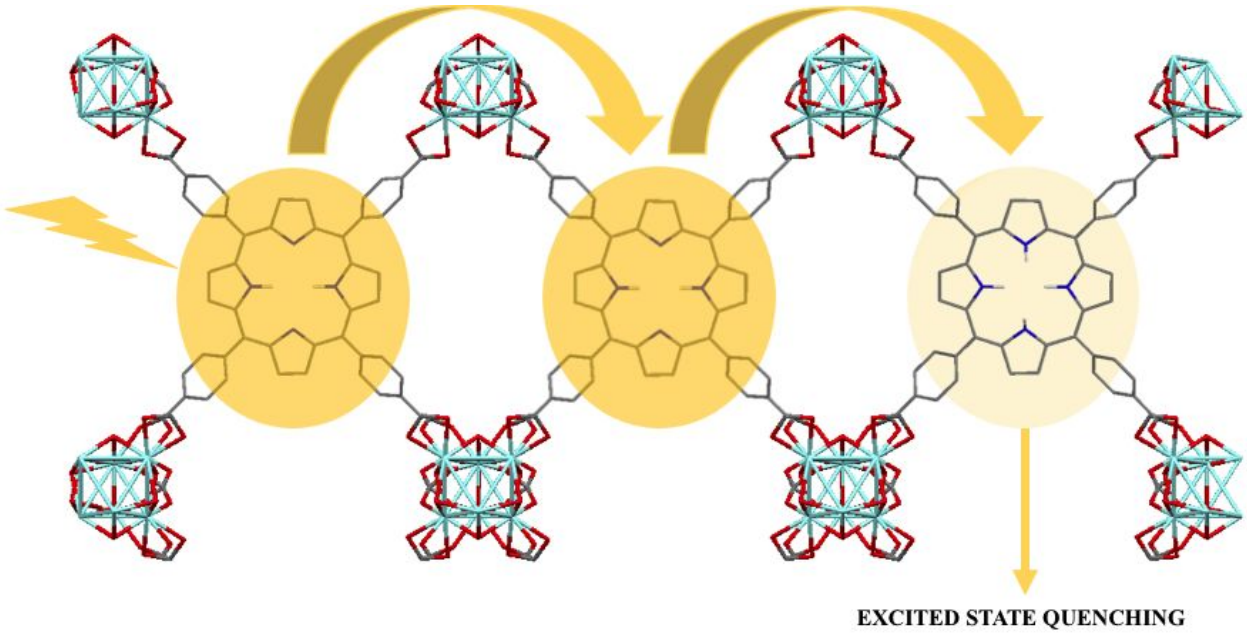
EXCITED STATE QUENCHING

TOC GRAPHIC